# HIGH-RESOLUTION NEAR-INFRARED IMAGING OF THE ORION 114−426 SILHOUETTE DISK

MARK J. McCAUGHREAN,[1] HUA CHEN,[2] JOHN BALLY,[3] ED ERICKSON,[4] RODGER THOMPSON,[2] MARCIA RIEKE,[2]
GLENN SCHNEIDER,[2] SUSAN STOLOVY,[2] AND ERICK YOUNG[2]

## ABSTRACT

We present the first high-resolution near-infrared images of the edge-on silhouette circumstellar disk, Orion 114−426, made using NICMOS on the *Hubble Space Telescope*. Images taken against the bright nebular background of the ionized hydrogen Paα line at 1.87 μm show the major axis of the disk to be approximately 20% smaller than at 0.6 μm, from which we deduce the structure of the edge of the disk. Continuum images of diffuse polar lobes above and below the plane of the disk show a morphology and evolution with wavelength consistent with predictions for reflection nebulae in a diffuse envelope with large polar cavities, surrounding a thin, massless, Keplerian disk, centered on an otherwise hidden central star. We make use of our observations and reasonable assumptions about the underlying disk structure to show that the disk mass is at least 10 $M_\oplus$ and plausibly $\geq 5 \times 10^{-4} M_\odot$.

*Subject headings:* accretion, accretion disks — circumstellar matter — infrared: ISM: continuum —
infrared: ISM: lines and bands — ISM: individual (Orion Nebula) — stars: formation

## 1. INTRODUCTION

The discovery of a family of circumstellar disks seen as dark silhouettes in projection against the Orion Nebula using the *Hubble Space Telescope* provided strong confirmation of the disk paradigm of star formation (O'Dell, Wen, & Hu 1993; O'Dell & Wen 1994; McCaughrean & O'Dell 1996, hereafter MO96). The disks range in diameter from 50 to 1000 AU, and thus the ∼50 AU (0″.1 at 450 pc) resolution of the *HST* observations was sufficient to examine their structure directly at optical wavelengths. An important finding was that the radial surface density profiles appear to be abruptly truncated at some outer radius, perhaps due to external effects from the surrounding H II region and dense cluster (MO96). More detailed examination of this transition zone should lead to a greater understanding of the evolution of disks in harsh environments.

The discovery images were obtained over a relatively narrow wavelength range (5007–6585 Å), and further insight should be possible using *HST* observations at shorter and longer wavelengths. In the blue/near-UV (∼2000–4000 Å), the spatial resolution approaches ∼15 AU, while increased dust opacity at these wavelengths should also allow more tenuous structures to be traced to larger radii. Conversely, the considerable reduction in dust opacity at near-IR wavelengths should allow us to trace structures to smaller radii, albeit with commensurately poorer spatial resolution. Consequently, we are conducting follow-up *HST* studies from the near-UV to near-IR (0.3–2.5 μm), and, in the present paper, we report preliminary near-IR observations using NICMOS of one silhouette disk, Orion 114−426. The largest of the sample at ∼1000 AU diameter, this disk is seen near edge-on, and, while the central star is not directly visible at optical wavelengths, its presence is betrayed by two polar nebulosities believed to be illuminated by it.

## 2. OBSERVATIONS

A comprehensive General Observer program (McCaughrean et al.; GO 7367) studying the Orion silhouette disks with NICMOS, STIS, and WFPC2 is being carried out during *HST* cycle 7. Early release observations using NICMOS were subsequently proposed by the Instrument Development Team (Erickson et al.; SM2/ERO 7114) for scientific verification and media use. Because of this overlap, the ERO data were reduced and analyzed collaboratively, resulting in studies of Orion 114−426 (presented here) and of the 182−413/183−419 field (Chen et al. 1998).

NICMOS observations of the Orion 114−426 field were obtained on 1997 April 19 during the Servicing Mission Orbital Verification following installation on the *HST*. Images were taken through broadband, narrowband, and polarimetric filters between 1 and 2.1 μm, as summarized in Table 1. Data reduction combined standard ground-based near-IR imaging techniques with parts of the NICMOS calibration pipeline. Multiple readouts combined with multiple positions on the sky were used to reject cosmic-ray events; electronic offsets were removed with on-orbit dark images; quantum efficiency variations were removed with flat fields taken on-orbit where possible, and otherwise from ground tests. Finally, mosaics were made registering the multiple images using stars or *HST* pointing information. Detailed photometric calibration was not attempted, but ground-based near-IR magnitudes for stars in the field were used to calibrate within ±0.2 mag.

Despite integration times significantly shorter than those planned for the GO program, important preliminary results were nevertheless obtained from the narrowband imaging against the bright Paα background at 1.87 μm, broadband imaging at 1.1 and 1.6 μm, and the polarization imaging at 2.0 μm. The three polarizer position images were combined to form a 2 μm continuum image, but because of remaining uncertainties in the correct analysis techniques for NICMOS polarimetry and incomplete on-orbit polarization calibration, the polarization results themselves are deferred to a future paper. The remaining narrowband images did not provide useful additional information and are not further discussed.

[1] Max-Planck-Institut für Radioastronomie, Auf dem Hügel 69, 53121 Bonn, Germany; mjm@mpifr-bonn.mpg.de.
[2] Steward Observatory, University of Arizona, 933 N. Cherry Avenue, Tucson, AZ 85721.
[3] Center for Astrophysics and Space Astronomy, University of Colorado, Boulder, CO 80309–089.
[4] NASA Ames Research Center, MS 245–6, Moffett Field, CA 94035–1000.

TABLE 1
OBSERVATION LOG

| Camera[a] | Filter[b] | Integration[c] (s) | Notes |
|---|---|---|---|
| NIC2 ...... | POL0L | 384 | 1.9–2.1 $\mu$m, 0° polarizer |
| NIC2 ...... | POL120L | 384 | 1.9–2.1 $\mu$m, 120° polarizer |
| NIC2 ...... | POL240L | 384 | 1.9–2.1 $\mu$m, 240° polarizer |
| NIC2 ...... | F212N | 384 | 2.121 $\mu$m, 1% wide, $H_2$ $v = 1$–0 $S(1)$ line |
| NIC2 ...... | F215N | 384 | 2.150 $\mu$m, 1% wide, continuum |
| NIC1 ...... | F110W | 384 | 0.8–1.4 $\mu$m |
| NIC1 ...... | F160W | 384 | 1.4–1.8 $\mu$m |
| NIC1 ...... | F164N | 288 | 1.644 $\mu$m, 1% wide, [Fe II] line |
| NIC1 ...... | F166N | 288 | 1.650 $\mu$m, 1% wide, continuum |
| NIC1 ...... | F187N | 288 | 1.875 $\mu$m, 1% wide, Pa$\alpha$ line |
| NIC1 ...... | F190N | 288 | 1.900 $\mu$m, 1% wide, continuum |

[a] NIC2 image scale 0″.0757 pixel⁻¹, field of view 19″.2 × 19″.2; NIC1 image scale 0″.0432 pixel⁻¹, field of view 11″.0 × 11″.0.

[b] Standard *HST* nomenclature for filter names used.

[c] Total integration time, in each case split into three subimages at slightly dithered positions, each taken using NICMOS MULTIACCUM integration sequences for improved signal-to-noise ratio and cosmic-ray rejection.

## 3. RESULTS

### 3.1. *Narrowband Imaging in* Pa$\alpha$

The highest S/N images of the silhouettes obtained by MO96 were through a narrowband H$\alpha$ (6565 Å) filter, admitting the full emission-line flux from the bright Orion Nebula H II region, while minimizing continuum emission from the central stars, or in the case of Orion 114−426, its polar lobes. The brightest near-IR counterpart is the Pa$\alpha$ line at 1.87 $\mu$m, which cannot be detected from the ground due to atmospheric absorption. For typical H II region ionization parameters ($10^4$ K, $10^4$ cm⁻³, case B) and $A_V \sim 1$ mag foreground to the nebula, the detected photon flux at Pa$\alpha$ should be ~60% of that at H$\alpha$; the brightest equivalent line available to ground-based observers (Br$\gamma$ at 2.16 $\mu$m) would be a further factor of 10 fainter (Osterbrock 1989).

The Pa$\alpha$ 1.87 $\mu$m image of Orion 114−426 is shown in Figure 1 (Plate L42) with the H$\alpha$ (6565 Å) image from MO96. The S/N in the Pa$\alpha$ image is poor ($\lesssim$5:1) since the integration time was short (288 s), and the NIC1 image scale of 0″.0432 pixel⁻¹ overresolved the 0″.19 FWHM diffraction-limited resolution of the telescope at 1.87 $\mu$m.

Nevertheless, the silhouette is clearly detected, allowing a preliminary measurement of its size. The data were binned by a factor of 2 to better match the appropriate pixel size (i.e., 2 pixels per FWHM) and were then averaged across the minor axis. The resulting one-dimensional major-axis profile had high enough S/N to show the two ends of the disk as sharp dips separated by 1″.8. As discussed in detail by MO96, the apparent size and structure of a silhouette disk is a convolution of its real form with the instrumental point spread function, and, following MO96, we adjusted the parameters of a model edge-on disk convolved with a model *HST*+NICMOS PSF calculated using the Tiny Tim software (Krist & Hook 1997) until the major-axis length was reproduced. The resulting best-fit model disk has a major-axis size of $\simeq$800 AU at 1.87 $\mu$m, ~20% less than the 1012 AU measured at 0.6 $\mu$m (MO96). The same procedure used on the 2 $\mu$m continuum image (§ 3.2) yielded the same result to within 5%. Finally, we verified the overall procedure by degrading the high S/N [O III] image from MO96 to the same spatial resolution and S/N as the Pa$\alpha$ image, and then performing the same fitting process, before retrieving the correct size for the disk at optical wavelengths.

### 3.2. *Continuum Imaging of the Polar Lobes*

The optical continuum image of Orion 114−426 showed faint polar lobes, interpreted as reflection nebulae of tenuous dust above and below the plane of the disk, illuminated by the otherwise unseen central star (MO96). Similar reflection nebulae are seen above and below the plane of an edge-on disk in the HH 30 system (Burrows et al. 1996). The wavelength-dependent morphology and polarization structure of the lobes in Orion 114−426 should allow us to probe the underlying form of the disk, the geometry of polar cavities, the grain size, and scattering function.

The near-IR broadband continuum images, along with the F547M image from MO96, are shown in Figure 2 (Plate L43) in gray-scale and contour forms. As the wavelength increases, three effects are seen. First, the initially fainter SE polar lobe increases in brightness until it equals and then outshines the intensity of the NW lobe. The peak intensities in the lobes (after background subtraction) are in the ratios 7.3:1, 2.2:1, 1.2:1, and 0.85:1 for the NW:SE lobes, at 0.57, 1.1, 1.6, and 2.0 $\mu$m, respectively. Second, the nebulae move closer together, as the reduced extinction allows us to probe closer to the disk midplane; the separations of the peak pixels in the two lobes are at 0″.64, 0″.43, 0″.40, and 0″.32 at 0.57, 1.1, 1.6, and 2.0 $\mu$m, respectively. Third, the nebulae appear to flatten from conical to slablike.

These features can be compared to model disks and envelopes (see, e.g., Lazareff, Pudritz, & Monin 1990; Whitney & Hartmann 1992 [hereafter WH92], 1993 [hereafter WH93]; Fischer, Henning, & Yorke 1996, hereafter FHY96). The general broad fan shape and increasing flatness of the nebulae are best reproduced by model SH of FHY96, i.e., a thin, massless disk (in comparison to the central star) in Keplerian rotation, with an envelope and broad polar cavities. Models with thick, massive disks have more polar material and result in images with too much elongation perpendicular to the disk. The same is true of models with just a narrow, cylindrical polar hole rather than a broader, so-called "streamline" cavity (WH93).

Since the central star in Orion 114−426 is not seen, the disk must lie within a few degrees of edge-on, as the thin disk of the SH model does not occult the central star unless this condition is met (FHY96). This degree of alignment is also argued for on the grounds that the two lobes have nearly equal bright-

ness in the near-IR. The asymmetry between the two lobes in the optical continuum (Fig. 2a) can probably explained by asymmetries in the outer, more diffuse parts of the envelope, perhaps due to external effects in the H II region.

## 4. DISCUSSION

### 4.1. *Disk Structure*

The disk appears ∼20% smaller at 1.87 $\mu$m than at 0.6 $\mu$m, and thus we are clearly resolving structure in its outer parts. In order to understand the implications of these observations, we need to examine the theoretical expectations. For a thin, massless, Keplerian disk that is hydrostatically supported and vertically isothermal (Shakura & Sunyaev 1973; Pringle 1981; Lazareff et al. 1990), the density $\rho$ as a function of radius, $r$, and height above the midplane, $z$, is

$$\rho(r, z) = \rho_d \left(\frac{r}{r_d}\right)^{-15/8} \exp\left\{-\frac{\pi}{4}\left[\frac{z}{h(r)}\right]^2\right\}, \quad (1)$$

where $\rho_d$ is the midplane density at the outer disk radius, $r_d$, and $h(r)$ is the disk scale height,

$$h(r) = z_d \left(\frac{r}{r_d}\right)^{9/8}, \quad (2)$$

where $z_d$ is the scale height at $r_d$. The disk surface density is then

$$\Sigma(r) = 2\rho_d z_d \left(\frac{r}{r_d}\right)^{-3/4}. \quad (3)$$

For typical Orion Nebula dust grains ($R = 5$; Cardelli, Clayton, & Mathis 1989), the extinction at 1.87 $\mu$m is one-sixth of that at 0.6 $\mu$m, and thus achieving the same effective optical depth requires 6 times higher column density at the longer wavelength. For a face-on disk with unity optical depth at 0.6 $\mu$m at 506 AU radius, equation (3) shows that the equivalent optical depth at 1.87 $\mu$m would occur at 46 AU, i.e., the disk would appear much smaller in the near-IR. For an edge-on disk, the calculation is harder: we are probing the midplane density of the disk, not the surface density, and the line of sight through the disk at a given "impact parameter" (i.e., the distance off-center) integrates over different densities at different radii. Assuming the disk is truncated at some outer radius, we can integrate the total column density through the midplane as a function of the impact parameter $a$. We have calculated profiles for disks in which the midplane density scales as $r^\alpha$, with $\alpha = -1$, $-2$, and $-3$ (Fig. 3). These values were chosen since simple analytical integrals exist in each case, but they also closely correspond to plausible disk models: $\alpha = -9/8 \simeq -1$ would yield a surface density independent of radius; $\alpha = -15/8 \simeq -2$ yields the canonical $\Sigma(r) \propto r^{-3/4}$; $\alpha = -21/8 \sim -3$ yields $\Sigma(r) \propto r^{-3/2}$, a commonly assumed density law for more massive circumstellar disks (cf. Adams, Shu, & Lada 1988).

Rough power laws can be fitted to the inner section of each curve in Figure 3, with the column density increasing as $a^\gamma$, and $\gamma \simeq -1/4$, $-1$, and $-2$ corresponding to $\alpha = -1$, $-2$, and $-3$, respectively. In the canonical case of $\alpha = -2 \simeq -15/8$, a disk with unity optical depth at 506 AU at 0.6 $\mu$m would have the same optical depth at 84 AU at 1.87 $\mu$m. Thus, even
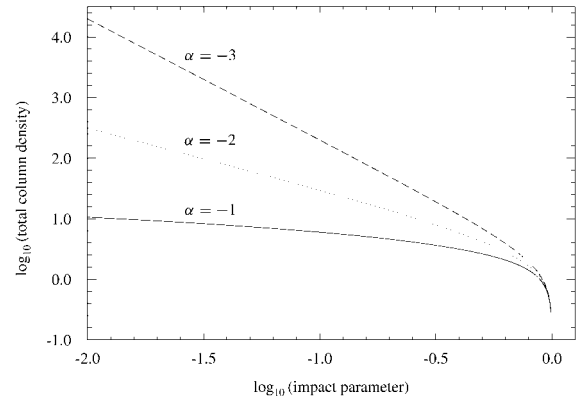


FIG. 3.—Model midplane column density profiles for an edge-on disk with an outer edge at unity radius. The total integrated column density (in arbitrary units) is shown as a function of the impact parameter, i.e., the distance off-center at which the column is being measured. The three curves correspond to underlying radial power-law density distributions of the midplane density with $\rho \propto r^\alpha$, with $\alpha = -1$, $-2$, and $-3$. See text for further details.

though an edge-on disk will shrink less with wavelength than a face-on one, it is clear that for Orion 114−426, the observed decrease in size of only 20% (i.e., −0.1 dex) for an increase in density of 6 (i.e., 0.78 dex) would require $\gamma \sim -8$, and thus $\alpha \sim -9$ and $\Sigma(r) \propto r^{-8}$, quite inconsistent with conventional understanding of disk structure.

The exception comes near the edge of a disk, where the integrated column density rises sharply as the path length increases most rapidly. Indeed, Figure 3 shows that in the $\alpha = -2$ case, the density *does* increase by the required factor of 6 within 80% of the outer radius, as observed. Thus, the observed shift between the optical edge at 506 AU and the infrared edge at 400 AU could still be consistent with the midplane density following the canonical power law for a thin, massless disk, *as long as* the disk is physically truncated somewhere near the optical edge. As discussed by MO96, it seems plausible that the disk may be truncated due to physical processes present in the Orion Nebula H II region and/or Trapezium Cluster, and it may be possible to ascertain which particular process is responsible from our future *HST* observations, which will trace the radial structure of Orion 114−426 over a full order of magnitude in limiting column density.

### 4.2. *The Disk Mass Revisited*

The mass of the Orion 114−426 disk remains unknown. In particular, does it exceed the ∼0.01 $M_\odot$ of the minimum mass solar nebula (MMSN), i.e., is it massive enough to form a planetary system similar to our own? O'Dell & Wen (1994) and MO96 discuss how the mass of a silhouette disk can be roughly estimated, noting that the minimum intensity seen toward it is typically ∼10% of that of the background H II region. Assuming this to be background emission attenuated by the disk, a line-of-sight column density is calculated for each point in the silhouette, and, summing over the whole disk area, a total mass is estimated. However, virtually all of this "disk light" is an artifact, as the background emission is blended into the disk by the instrumental PSF (MO96). Thus, the usefulness of the "transmission technique" is diminished, but it at least provides an absolute *lower limit* mass, an important counterpoint to the results from millimeter interferometry that, as yet, generally provide only *upper limit* masses for disks in the Tra-

pezium Cluster (Mundy, Looney, & Lada 1995; Lada et al. 1996).

MO96 used the transmission technique to estimate lower limit masses for the six silhouette disks based on their optical images. The masses were small, typically several orders of magnitude less than the MMSN. The most massive was Orion $114-426$ at $0.002$ $M_\odot$, but we must report here that an error was made in calculating the area and thus mass of Orion $114-426$ in MO96: its minimum mass should be revised downward to $2 \times 10^{-4}$ $M_\odot$. (The masses for the other disks given in Table 2 of MO96 remain unaffected by this error.)

In principle, the transmission technique could be applied to our new near-IR images of Orion $114-426$, resulting in a significantly *higher* estimate of the minimum mass. Since the disk is only marginally smaller at $1.87$ $\mu$m, the reduced near-IR extinction should lead to a higher mass, on the order of the factor of 6 in $A_V/A_{1.87\,\mu m}$. However, the present images are not good enough to make such estimates: the Pa$\alpha$ image has very poor S/N, making a reliable measure of the disk/background flux ratio impossible, and, while the continuum images have much higher S/N, the silhouette is contaminated by the reflection nebulae, making it difficult to measure the underlying disk/background flux ratio and the true silhouette area. Such calculations must wait until higher quality Pa$\alpha$ data are available.

In the interim, alternative approaches to estimating the disk mass can be taken. The nondetection of the central star in the POL 2 $\mu$m continuum image can be used to set a lower limit on the total column density through the disk midplane, depending on the intrinsic brightness of the star. The integrated flux from the two reflection nebulae is $K = 14.5$ mag, which clearly only represents a fraction of the flux we would see from the central star if it had no disk. Some estimate of this fraction can be made from WH92 and WH93, who tabulate $F/F_\star$ (the total flux observed as a fraction of the flux that would be seen if the star had no disk or envelope) for a variety of models. While $F/F_\star$ ranges from 0.01%–10% depending on the disk and envelope structure, inclination angle, grain properties, and total opacity, $\sim 1\%$ is typical for models inferred for Orion $114-426$ (i.e., near edge-on flared disk, e.g., WH92 models 3 and 4 with $\mu < 0.3$, perhaps with a tenuous envelope with broad polar cavities, e.g., WH93 models 5–8). The inferred intrinsic brightness of the central star is then $K \sim 9.5$ mag, corresponding to a 1 Myr old, $\sim 1.5$ $M_\odot$ star at 450 pc (D'Antona & Mazzitelli 1994). Since the star is undetected in the 2 $\mu$m image to a 5 $\sigma$ point source detection limit of $K = 18.8$ mag, the implied line-of-sight extinction toward it is $\geq 9.3$ mag at 2 $\mu$m, or $A_V \geq 60$ mag. Assuming the disk is exactly edge-on, the corresponding column density through the disk midplane to the central star is $\geq 1.1 \times 10^{23}$ cm$^{-2}$ (assuming $1 A_V \equiv 1.9 \times 10^{21}$ cm$^{-2}$).

The disk outer radius, $r_d = 506$ AU, is known from the data of MO96. The same data can be used to determine $z_d$, the scale height at $r_d$: we fitted a one-dimensional average minor axis profile across the [O III] image of Orion $114-426$ (Fig. 4 of MO96) with a Gaussian characterized by equation (2), yielding $z_d = 72$ AU. Finally, we assume the disk inner radius, $r_i = 1$ AU; since the surface density increases toward the center with a power less than 1, our results are not too sensitive to this assumption. Integrating equation (1) (with $\alpha = -15/8$) through the midplane, we calculate the midplane density at the outer edge, $\rho_d \geq 5.8 \times 10^4$ cm$^{-3}$. Then integrating equation (3) between $r_d$ and $r_i$, the total number of particles (H I + 2H$_2$) is

$\geq 3.4 \times 10^{52}$, yielding a mass estimate of $\geq 5.7 \times 10^{28}$ g or $\geq 10$ $M_\oplus$.

Although it is clear that very little mass is required to render the central star invisible, the disk mass is likely to be significantly greater. Using the analytical solution for the total column density seen through the midplane of an edge-on disk in the $\alpha = -2 \simeq -15/8$ case (§ 4.1), and assuming $\rho_d = 5.8 \times 10^4$ cm$^{-3}$ at an outer radius of 506 AU, we obtain values $\sim 2 \times 10^{20}$ cm$^{-2}$ or $A_V \sim 0.1$ mag just inside the edge. Yet the disk must have a significantly higher column density there to be *seen* as an edge: the results of MO96 show that the attenuation at the edge of the disk is at least 85%, equivalent to $A_V \geq 2$ mag, in turn implying $\rho_d \geq 1.2 \times 10^6$ cm$^{-3}$. This is a plausible value if (for example) the location of the disk edge is set by pressure balance with the surrounding H II region: assuming a temperature and density for the latter of $10^4$ K and $10^4$ cm$^{-3}$ and an outer disk temperature of 10–100 K, densities at the disk edge of $10^6$–$10^7$ cm$^{-3}$ would be predicted.

Inserting $\rho_d \geq 1.2 \times 10^6$ cm$^{-3}$ into equation (3) along with our other derived disk parameters yields a disk mass of $\geq 1.1 \times 10^{30}$ g or $\geq 5 \times 10^{-4}$ $M_\odot$. While still considerably less than the MMSN, this is a lower limit, and the disk might be more massive. However, our present simple calculations based on lower limit extinction measurements alone cannot be pushed much further. Burrows et al. (1996) have shown for HH 30 that more realistic mass estimates can be made by fitting the structure of the polar reflection nebulae, in particular the width of the dark lane of obscuration between them, and such an approach will be taken with Orion $114-426$ when our higher S/N and resolution cycle 7 *HST* data are available. Ultimately, the most meaningful estimate of disk mass must come from measurements of optically thin tracers at millimeter wavelengths: such observations have been obtained for Orion $114-426$ and will be discussed in a future paper.

## 5. CONCLUSIONS

We have presented preliminary NICMOS images of the Orion $114-426$ circumstellar disk. The disk appears to be roughly 20% smaller at $1.87$ $\mu$m than at $0.6$ $\mu$m, which we attribute to a standard radial power-law density distribution inside a heavily truncated edge to the disk at $\sim 500$ AU radius. The general wavelength-dependent morphology of the polar lobes is consistent with models of a thin, massless disk surrounded by a tenuous envelope with broad polar cavities, and their flux was used as an indirect way of estimating the mass of the central star to be 1.5 $M_\odot$. The nondetection of the star at 2 $\mu$m was then used to estimate the minimum total column density through the disk midplane, and thus a minimum disk mass of $\geq 10$ $M_\oplus$, assuming that it follows the standard form for a massless disk in Keplerian rotation. The hard edge of the disk was used to improve the lower limit estimate under similar assumptions, resulting in a mass $\geq 5 \times 10^{-4}$ $M_\odot$.

## REFERENCES

Adams, F. C., Shu, F. H., & Lada, C. J. 1988, ApJ, 326, 865
Burrows, C. J., et al. 1996, ApJ, 473, 437
Cardelli, J. A., Clayton, G. C., & Mathis, J. S. 1989, ApJ, 345, 245
Chen, H., Bally, J., O'Dell, C. R., McCaughrean, M. J., Thompson, R. I., Rieke, M. J., Schneider, G., & Young, E. T. 1998, ApJ, 492, L173
D'Antona, F., & Mazzitelli, I. 1994, ApJS, 90, 467
Fischer, O., Henning, T., & Yorke, H. 1996, A&A, 308, 863 (FHY96)
Krist, J., & Hook, R. 1997, Tiny Tim User Manual Version 4.3 (Baltimore: STScI)
Lada, E. A., Dutrey, A., Guilloteau, S., & Mundy, L. G. 1996, BAAS, 189, 53.01

Lazareff, B., Pudritz, R. E., & Monin, J.-L. 1990, ApJ, 358, 170
McCaughrean, M. J., & O'Dell, C. R. 1996, AJ, 111, 1977 (MO96)
Mundy, L. G., Looney, L. W., & Lada, E. A. 1995, ApJ, 452, L137
O'Dell, C. R., & Wen, Z. 1994, ApJ, 436, 194
O'Dell, C. R., Wen, Z., & Hu, X. 1993, ApJ, 410, 696
Osterbrock, D. E. 1989, Astrophysics of Gaseous Nebulae and Active Galactic Nuclei (Mill Valley: University Science Books), 84
Pringle, J. E. 1981, ARA&A, 19, 137
Shakura, N. I., & Sunyaev, R. A. 1973, A&A, 24, 337
Whitney, B. A., & Hartmann, L. 1992, ApJ, 395, 529 (WH92)
———. 1993, ApJ, 402, 605 (WH93)

(a) F656N: Hα

N
E
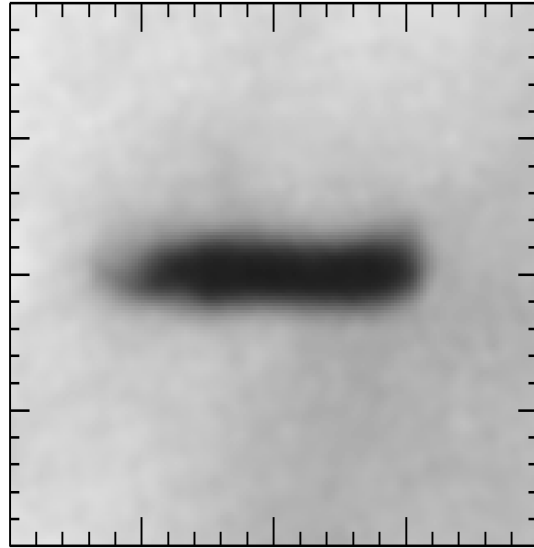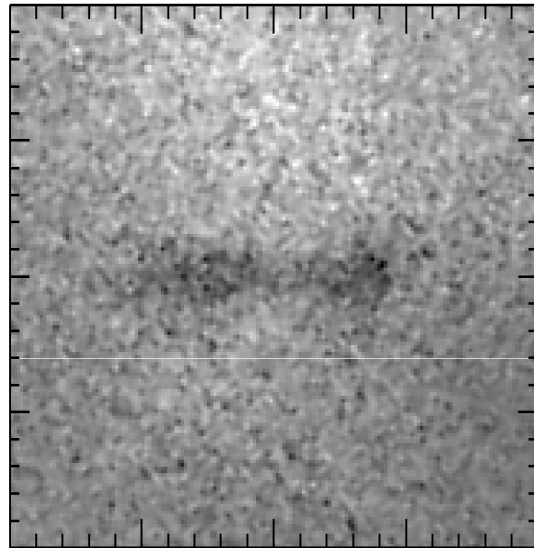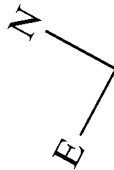
(b) F187N: Paα

FIG. 1.—Emission-line images of the Orion 114−426 silhouette disk: (*a*) Hα 6565 Å, (*b*) Paα 1.87 μm. Both images have been magnified and rotated to a common scale and orientation. Each image is 4″ × 4″ in size or 1800 × 1800 AU at 450 pc. Major tick marks are at 1″ intervals. The intensity scaling is arbitrary.
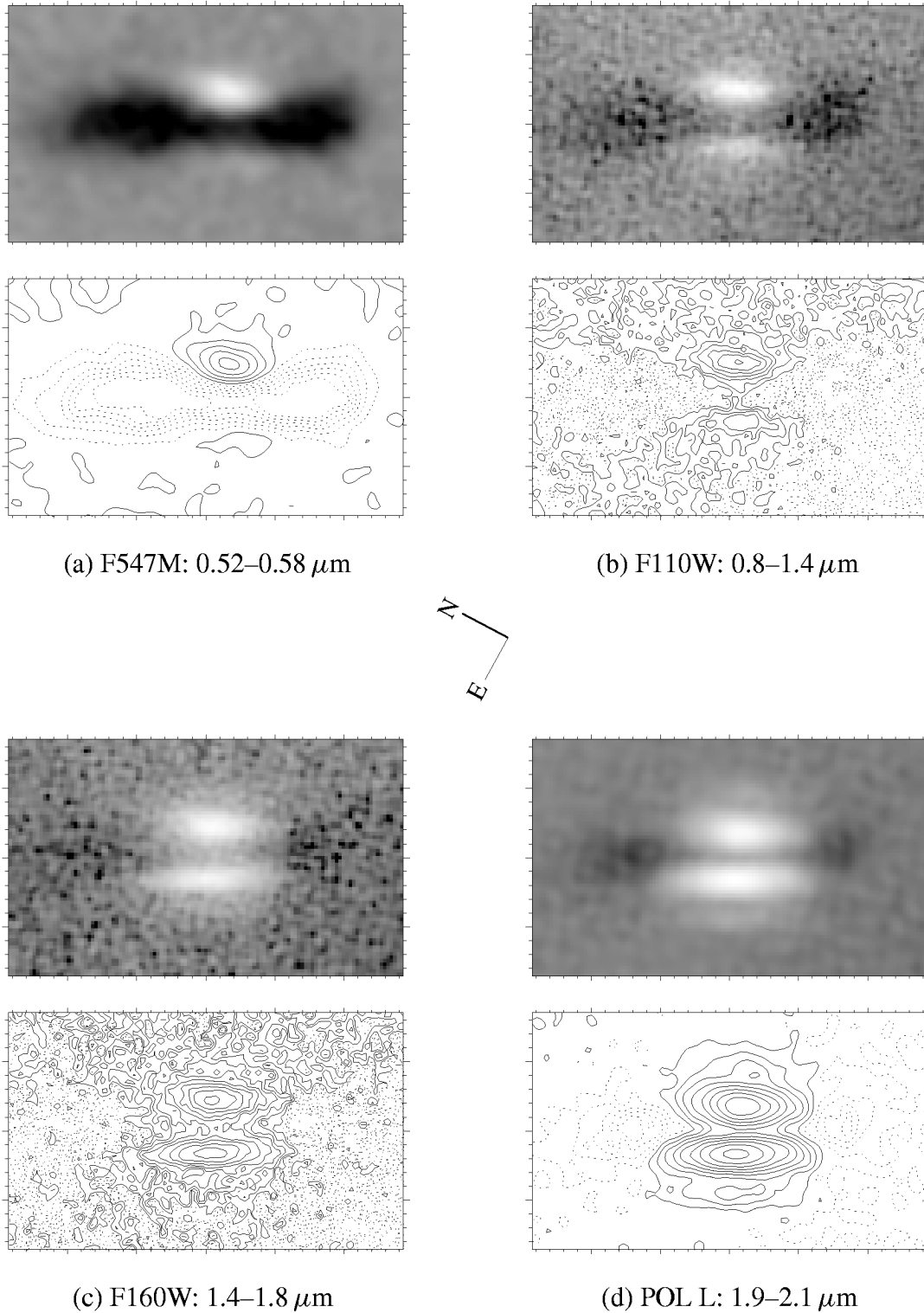
McCaughrean et al. (see 492, L158)

(a) F547M: 0.52–0.58 $\mu$m

(b) F110W: 0.8–1.4 $\mu$m

(c) F160W: 1.4–1.8 $\mu$m

(d) POL L: 1.9–2.1 $\mu$m

FIG. 2.—Continuum images of the Orion 114−426 disk and polar lobes in gray-scale and contour form: (*a*) F547M (0.52–0.58 $\mu$m); (*b*) F110W (0.8–1.4 $\mu$m); (*c*) F165W (1.4–1.8 $\mu$m); (*d*) intensity image derived from the POL0L/POL120L/POL240L polarization images (1.9–2.1 $\mu$m). All images have been magnified and rotated to a common scale and orientation. Each image is 2″86 × 1″71 in size or ∼1290 × 770 AU at 450 pc. Major tick marks are at 1″ intervals. The absolute intensity levels are arbitrary, but the contours are spaced by 0.1 dex. Contours below the local mean background tracing the silhouette disk are drawn as dashed lines. Note that the fainter "sidelobes" seen above and below the main nebulae in the POL L image are artifacts resulting from the diffraction PSF of the *HST* + NICMOS.

McCAUGHREAN et al. (see 492, L158)